

Planetesimal Formation by Gravitational Instability of a Porous-Dust Disk

Shugo Michikoshi¹, and Eiichiro Kokubo²

michikos@ccs.tsukuba.ac.jp, and kokubo@th.nao.ac.jp

ABSTRACT

Recently it is proposed that porous icy dust aggregates are formed by pairwise accretion of dust aggregates beyond the snowline. We calculate the equilibrium random velocity of porous dust aggregates taking into account mutual gravitational scattering, collisions, gas drag, and turbulent stirring and scattering. We find that the disk of porous dust aggregates becomes gravitationally unstable as they evolve through gravitational compression in the minimum-mass solar nebula model for a reasonable range of turbulence strength, which leads to rapid formation of planetesimals.

Subject headings: planetary systems: formation, planetary systems: protoplanetary disks

1. Introduction

In the standard scenario of planet formation, planetesimals are the building blocks of planets (e.g., Safronov 1969; Hayashi et al. 1985). In a protoplanetary disk small dust grains grow to km-sized objects called planetesimals. From planetesimals, protoplanets or planetary embryos form through a process of the runaway and oligarchic growth (e.g., Kokubo & Ida 1998, 2012). However, the formation mechanism of planetesimals is one of today’s most important unsolved problems.

In the classical model of planetesimal formation, the gravitational instability (GI) plays a key role. As dust particles grow large and decouple from gas, they settle onto the disk midplane and form a dust layer. When the density of the dust layer exceeds the Roche density, the GI occurs (Safronov 1969; Goldreich & Ward 1973; Hayashi et al. 1985). The gravitationally unstable dust disk fragments into gravitationally bound objects (Michikoshi et al. 2007, 2009, 2010). They finally become planetesimals as they shrink.

The above model assumes no turbulence in the gas disk. However, the turbulence is likely to be driven by the magneto-rotational instability (e.g., Sano et al. 2000) and the shear instability

¹ Center for Computational Sciences, University of Tsukuba, Tsukuba, Ibaraki 305-8577, Japan

² Division of Theoretical Astronomy, National Astronomical Observatory of Japan, Osawa, Mitaka, Tokyo 181-8588, Japan

(e.g., Sekiya & Ishitsu 2000; Michikoshi & Inutsuka 2006). Under the turbulence dust particles are stirred up and cannot settle onto the midplane (e.g., Weidenschilling & Cuzzi 1993). In the standard minimum mass solar nebular (MMSN) model, the GI does not occur (Sekiya 1998). One of the possible mechanisms for overcoming this difficulty is the streaming instability, which leads to the formation of the gravitationally bound objects (Youdin & Goodman 2005; Johansen et al. 2007).

Another formation model is the pairwise coagulation of dust particles. The recent studies on the dust growth showed that the icy dust aggregates formed by coagulation are not compact but significantly porous (Dominik & Tielens 1997; Blum & Wurm 2000; Wada et al. 2007, 2008, 2009; Suyama et al. 2008, 2012; Okuzumi et al. 2012). The internal density of dust aggregates is much smaller than the material density, which is $\sim 10^{-5} \text{ g cm}^{-3}$. Some compression mechanism is necessary to form compact planetesimals with $\sim 1 \text{ g cm}^{-3}$. Kataoka et al. (2013) found that the dust aggregates can be compressed by the ram pressure when the dust aggregate mass $m_d \lesssim 10^{11} \text{ g}$. The dust aggregates with $m_d \gtrsim 10^{11} \text{ g}$ are compressed by the self-gravity and finally the density reaches $\sim 0.1 \text{ g cm}^{-3}$.

In this paper, we revisit the final stage of the dust aggregate evolution by the gravitational compression. We investigate the dynamics of the porous dust aggregates and demonstrate that the GI takes place as a result of the dust evolution. In Section 2 we describe the calculation method. We present the results in Section 3. Section 4 is devoted to a summary and discussion.

2. Model and Method

2.1. Disk Model

We adopt the surface densities of gas and dust, $\Sigma_g = 1700 f_g (a/\text{AU})^{-3/2} \text{ g cm}^{-2}$ and $\Sigma_d = f_d \Sigma_g$, where a is the distance from the central star, f_g is the ratio to the MMSN model and $f_d = 0.018$ is the dust-to-gas mass ratio beyond the snowline (Hayashi 1981; Hayashi et al. 1985). We adopt the temperature profile $T = T_1 (a/\text{AU})^{-3/7} \text{ K}$, where $T_1 = 120$ (Chiang & Youdin 2010). The isothermal sound velocity is $c_s = \sqrt{k_B T / m_g}$, where k_B is the Boltzmann constant and $m_g = 3.9 \times 10^{-24} \text{ g}$ is the mean molecular mass. The gas density at the disk midplane is $\rho_g = \Sigma_g / (\sqrt{2\pi} c_s / \Omega)$, where $\Omega = \sqrt{GM_*/a^3}$ is the Keplerian frequency and M_* is the central star mass. We adopt $M_* = M_\odot$. The mean free path of gas molecules is $l = m_g / \sigma_g \rho_g$, where $\sigma_g = 2 \times 10^{-15} \text{ cm}^2$ is the collisional cross-section of gas molecules. The nondimensional radial pressure gradient is given as $\eta = -(1/2)[c_s/(a\Omega)]^2 \partial \log(\rho_g c_s^2) / \partial \log a$.

We consider the spherical porous dust aggregate with mass m_d and radius r_d , consisting of monomers with radius r_0 and density ρ_0 . As a first step, we assume that all the dust aggregates have the same mass (e.g., Kataoka et al. 2013). This assumption is justified if the size distribution has a steep single peak (e.g., Okuzumi et al. 2011, 2012). We define the mean internal density

$\rho_{\text{int}} = m_{\text{d}}/(4\pi r_{\text{d}}^3/3)$. The geometric cross-section of the dust aggregate is given as πr_{d}^2 .

2.2. Random Velocity of Dust Aggregates

We calculate the equilibrium random velocity v of dust aggregates considering gravitational scattering, collisions, and interaction with gas. For simplicity we assume the isotropic velocity distribution, that is, $v_x \simeq v_y \simeq v_z \simeq v/\sqrt{3}$, where v_x , v_y , and v_z are the x , y , and z components of the random velocity, respectively.

2.2.1. Gravitational Scattering

The random velocity increases by mutual gravitational scattering. The timescale of gravitational scattering is well described by Chandrasekhar’s relaxation time (Ida 1990). The heating rate due to gravitational scattering is

$$\left(\frac{dv^2}{dt}\right)_{\text{grav}} = n_{\text{d}}\pi\left(\frac{2Gm_{\text{d}}}{v_{\text{rel}}^2}\right)^2 v_{\text{rel}}v^2 \log \Lambda, \quad (1)$$

where $v_{\text{rel}} \simeq \sqrt{2}v$ is the typical relative velocity between dust aggregates, $n_{\text{d}} \simeq (\Sigma_{\text{d}}/m_{\text{d}})/(\sqrt{2\pi}v_z/\Omega)$ is the number density of dust aggregates, and $\Lambda = v_{\text{rel}}^2(v_z/\Omega + r_{\text{H}})/(2Gm_{\text{d}})$ where $r_{\text{H}} = (2m_{\text{d}}/3M_{\star})^{1/3}a$ is the Hill radius (Stewart & Ida 2000).

2.2.2. Collision

We assume that all collisions lead to accretion. Under this assumption the collisional damping rate is given as

$$\left(\frac{dv^2}{dt}\right)_{\text{col}} = -C_{\text{col}}n_{\text{d}}\pi(2r_{\text{d}})^2\left(1 + \frac{v_{\text{esc}}^2}{v_{\text{rel}}^2}\right)v_{\text{rel}}v^2, \quad (2)$$

where $v_{\text{esc}} = \sqrt{2Gm_{\text{d}}/r_{\text{d}}}$ is the surface escape velocity and C_{col} is the ratio of change of the kinetic energy on the collision. We consider that the orbit of the merged dust aggregate is given by that of the center of the mass and adopt $C_{\text{col}} = 1/2$ (Inaba et al. 2001).

2.2.3. Gas Effects

We consider the three interactions between turbulent gas and dust aggregates, namely, drag from the mean gas flow, turbulent stirring due to gas drag, and gravitational scattering by the turbulent density fluctuations.

The drag from the mean gas flow reduces v on the stopping timescale t_s as

$$\left(\frac{dv^2}{dt}\right)_{\text{gas,drag}} = -\frac{2}{t_s}v^2, \quad (3)$$

where t_s is

$$t_s = \frac{2m_d}{\pi C_D r_d^2 \rho_g u}, \quad (4)$$

where C_D is the dimensionless drag coefficient and u is the relative velocity between dust and gas. We adopt the typical relative velocity $u \simeq \sqrt{v^2 + \eta^2 v_K^2}$, where $v_K = a\Omega$ is the Keplerian velocity.

The gas drag law changes with r_d (e.g., Adachi et al. 1976). If $r_d \gtrsim l$, we use the Stokes or Newton drag. For the low Reynolds number case ($\text{Re} \ll 10^3$), the drag coefficient is approximated by $C_D \simeq 24/\text{Re}$ (Stokes drag), where $\text{Re} = 2r_d u/\nu$. The viscosity ν is given by $\nu = v_{\text{th}} l/2$ where $v_{\text{th}} = \sqrt{8/\pi} c_s$ is the thermal velocity. For the high Reynolds number case ($10^3 < \text{Re} < 2 \times 10^5$), the drag coefficient is almost constant $C_D \simeq 0.4\text{--}0.5$ (Newton drag). If $r_d \lesssim l$, we use the Epstein drag. Thus, we adopt the drag coefficient formula as (Brown & Lawler 2003)

$$C_D = \begin{cases} \frac{8v_{\text{th}}}{3u} & (r_d < 9l/4) \\ \frac{0.407}{1 + 8710/\text{Re}} + \frac{24}{\text{Re}}(1 + 0.150\text{Re}^{0.681}) & (r_d > 9l/4) \end{cases}. \quad (5)$$

In the turbulent gas, turbulence stirs dust aggregates by gas drag. In this case v reaches the equilibrium value (Youdin & Lithwick 2007)

$$v^2 = \frac{v_t^2 t_e}{t_e + t_s}, \quad (6)$$

where t_e is the eddy turnover time, $v_t = \sqrt{\alpha} c_s$ is the magnitude of the turbulent velocity, and α is the dimensionless turbulence strength (Cuzzi et al. 2001). Thus the heating rate due to turbulent stirring is

$$\left(\frac{dv^2}{dt}\right)_{\text{turb,stir}} = \frac{2\tau_e v_t^2 \Omega}{S(\tau_e + S)}, \quad (7)$$

where $\tau_e = t_e \Omega$ and $S = \Omega t_s$ is the Stokes number. We adopt $\tau_e = 1$ (Youdin 2011; Michikoshi et al. 2012).

The gas density fluctuates because of the turbulence. The dust aggregates are gravitationally scattered by the density fluctuations. Okuzumi & Ormel (2013) considered the magneto-rotational instability turbulence and derived the fitting formula of the heating rate

$$\left(\frac{dv^2}{dt}\right)_{\text{turb,grav}} = C_{\text{turb}} \alpha \left(\frac{\Sigma_g a^2}{M_*}\right)^2 \Omega^3 a^2, \quad (8)$$

where C_{turb} is the dimensionless factor that depends on the disk structure. We assume that the dead zone thickness is comparable to that of gas and adopt $C_{\text{turb}} = 3.1 \times 10^{-2}$ (Okuzumi & Ormel 2013).

2.2.4. Equilibrium Random Velocity

The evolution of v is described as

$$\frac{dv^2}{dt} = \left(\frac{dv^2}{dt}\right)_{\text{grav}} + \left(\frac{dv^2}{dt}\right)_{\text{col}} + \left(\frac{dv^2}{dt}\right)_{\text{gas,drag}} + \left(\frac{dv^2}{dt}\right)_{\text{turb,stir}} + \left(\frac{dv^2}{dt}\right)_{\text{turb,grav}}. \quad (9)$$

We can calculate the equilibrium random velocity of dust aggregates by setting $dv^2/dt = 0$.

2.3. Gravitational Instability Condition

To investigate the dynamical stability of the disk of dust aggregates, we use Toomre’s Q

$$Q = \frac{v_x \Omega}{3.36 G \Sigma_d}, \quad (10)$$

with the equilibrium random velocity (Toomre 1964). For the axisymmetric mode, the instability condition is $Q < 1$ (Toomre 1964). However, for $1 \lesssim Q \lesssim 2$, the non-axisymmetric mode or self-gravity wakes can grow on the dynamical timescale (e.g., Toomre 1981; Salo 1995; Michikoshi et al. 2007; Michikoshi & Kokubo 2016). Michikoshi et al. (2007, 2009, 2010) showed that the wakes fragment to form planetesimals. Therefore we adopt the condition $Q < Q_{\text{crit}} = 2$.

Note that in the regime of $Q \lesssim Q_{\text{crit}}$ near the evolution track of self-gravitational compression in our model (see Section 3.1), we obtain $S \gg 1$, and thus the secular GI reduces to the dynamical GI (Youdin 2011; Takahashi & Inutsuka 2014).

3. Results

3.1. Evolution of Dust Aggregates

We calculate v and then Q for a disk of porous dust aggregates with m_d and ρ_{int} . Figure 1 shows Q on the m_d - ρ_{int} plane for the fiducial model at 5 AU, where $f_g = 1$ and $\alpha = 10^{-3}$. We find a wide GI region with $Q < Q_{\text{crit}}$.

We consider the evolution of dust aggregates with $m_d \gtrsim 10^{11}$ g, where they are compressed by their self-gravity (Kataoka et al. 2013). Kataoka et al. (2013) investigated the evolution in this regime considering the compressive strength $P_{\text{comp}} = E_{\text{roll}} \rho_{\text{int}}^3 / r_0^3 \rho_0^3$ and the self-gravitational pressure $P_{\text{grav}} = G m_d^2 / \pi r_d^4$, where E_{roll} is the rolling energy. We draw the evolution track of dust aggregates in Figure 1, assuming $E_{\text{roll}} = 4.74 \times 10^{-9}$ erg, $\rho_0 = 1.0 \text{ g cm}^{-3}$, and $r_0 = 0.1 \mu\text{m}$. The evolution track crosses the GI region. In other words, the porous-dust disk becomes gravitationally unstable to fragment to form planetesimals.

Figure 2 shows the main heating and cooling mechanisms of the dust disk in the fiducial model. On the evolution track for $m_d \lesssim 10^{14}$ g, the main heating mechanism is turbulent stirring. Along

the evolution, r_d increases with m_d as $r_d \propto m_d^{1/5}$. For the Stokes drag, S ($\propto m_d/r_d$) increases with m_d . As S increases, dust aggregates decouple from turbulent gas, which reduces their random velocity. Therefore, Q decreases with increasing m_d and finally becomes less than Q_{crit} .

Figure 3a shows the various timescales. We calculate the timescales assuming the evolution track of the self-gravitational compression. The growth time for $S > 1$ is $t_{\text{grow}} = m_d/(\rho_d \pi r_d^2 v)$ where $\rho_d = m_d n_d$ and we neglect gravitational focusing. The radial drift time is given as $t_{\text{drift}} = a/(2S\eta v_K/(1 + S^2))$ (Adachi et al. 1976; Weidenschilling 1977). The GI timescale is about $t_{\text{GI}} \sim \Omega^{-1}$. The GI is much faster than the other processes. Thus the GI takes place once the GI condition is satisfied. The mass evolution of dust aggregates is shown in Figure 3b. The GI immediately forms planetesimals from dust aggregates. Note that the growth time here is under the assumption of perfect accretion for the sake of simplicity. The realistic growth of such huge porous dust aggregates is poorly understood.

3.2. Disk Condition for Gravitational Instability

We investigate the disk condition for the GI. Figure 4a represents the dependence of the GI region on α on the m_d - ρ_{int} plane. The GI region with $\alpha = 10^{-4}$ is larger than that in the fiducial model. Because the turbulence is the main source to increase the random velocity, v is smaller for smaller α . Therefore, the GI region expands. On the other hand, for $\alpha = 10^{-2}$, the GI region shrinks. The strong turbulence suppresses the GI. Figure 4b represents the dependence on f_g . The GI region is wider for larger f_g . For the massive disk, the GI more easily takes place.

We examine if the GI occurs along the dust evolution for disks with various f_g and α . The results are summarized in Figure 5a. As expected, the GI is more prone to occur for larger f_g and smaller α . In the MMSN model ($f_g = 1$), α should be less than 7×10^{-3} for the GI. If $f_g \gtrsim 1.3$, even though the strong turbulence case ($\alpha = 10^{-2}$), the GI is possible.

Next, we examine the dependence on a with the MMSN model ($f_g = 1$). Figure 5b shows the results. We find that the occurrence of the GI barely depends on a . The GI region exists for any a if $\alpha \lesssim 1 \times 10^{-2}$. The upper bound of α for the GI, where the GI region exists and the evolution track touches it, slightly decreases with increasing a . However, its dependence is weak. For $\alpha \lesssim 5 \times 10^{-3}$, the GI occurs for $a < 20$ AU.

In all the cases where the dust evolution leads to the GI in Figure 5, $t_{\text{GI}} < t_{\text{grow}}$ and $t_{\text{GI}} < t_{\text{drift}}$ are satisfied if the dust aggregates evolve by the self-gravitational compression. Thus the GI is inevitable on the course of dust evolution for the above disk conditions.

3.3. Critical Turbulence Strength

We derive the condition for the existence of the GI region as a function of disk parameters. In Figure 2, on the lower left boundary of the GI region, the main heating mechanism is turbulent stirring and the main cooling mechanism is collisional damping. Thus, we calculate v from $(dv^2/dt)_{\text{turb, stir}} + (dv^2/dt)_{\text{col}} = 0$ assuming $t_s \gg t_e$ and $u \simeq \eta v_K$ and neglecting gravitational focusing. We obtain the condition for $Q < Q_{\text{crit}}$ as

$$m_d \gtrsim m_{\text{low}} = 9.52 \times 10^{-8} \frac{\alpha^3 C_D^6 \eta^6 v_K^6 c_s^6 \rho_g^6 \tau_e^3}{C_{\text{col}}^3 Q_{\text{crit}}^6 \rho_{\text{int}}^2 \Sigma_d^9 G^6}. \quad (11)$$

On the upper right boundary of the GI region, the main heating source is turbulent scattering and the main cooling source is collisional damping. Thus, we calculate v from $(dv^2/dt)_{\text{turb, grav}} + (dv^2/dt)_{\text{col}} = 0$. The condition for the GI in this regime is

$$m_d \lesssim m_{\text{high}} = 4.10 \times 10^6 \frac{C_{\text{col}}^3 Q_{\text{crit}}^6 \Sigma_d^9}{\alpha^3 C_{\text{turb}}^3 \rho_{\text{int}}^2 \Sigma_g^6}. \quad (12)$$

As shown in Figure 2, these two conditions agree well with the numerical results. Thus, the necessary condition for the existence of the GI region is $m_{\text{low}} < m_{\text{high}}$. From this, we derive the critical α as

$$\alpha < \alpha_{\text{cr}} = 4.70 \times 10^2 \frac{C_{\text{col}} Q_{\text{crit}}^2 a^2 \Sigma_d^3}{\sqrt{C_{\text{turb}} \tau_e C_D \eta M_* \Sigma_g^2}}. \quad (13)$$

Using the disk model, we rewrite α_{cr} as

$$\alpha_{\text{cr}} = 1.38 \times 10^{-2} \tau_e^{-1/2} f_g \left(\frac{f_d}{0.018} \right)^3 \left(\frac{T_1}{120} \right)^{-1} \left(\frac{C_{\text{turb}}}{3.1 \times 10^{-2}} \right)^{-1/2} \left(\frac{Q_{\text{crit}}}{2} \right)^2 \left(\frac{a}{5 \text{ AU}} \right)^{-1/14}, \quad (14)$$

where we adopt $C_D = 0.5$. The dependence of α_{cr} on a is very weak. Therefore, the important disk parameters for the GI are f_g , f_d and T_1 . We plot α_{cr} in Figure 5, which agrees well with the numerical results.

The sufficient condition for the GI is that the dust evolution track crosses the GI region. We can numerically calculate the critical α for the sufficient condition. In our parameter regime $3 \text{ AU} < a < 20 \text{ AU}$ and $f_g > 1$, we empirically find that the critical α for the sufficient condition is slightly smaller than that for the necessary condition as shown in Figure 5. The difference is about 50% at a maximum. Note that the dust evolution track changes with monomer properties such as r_0 , ρ_0 , and E_{roll} .

4. Summary and Discussion

We have investigated the stability of the dust disk consisting of porous icy dust aggregates using their equilibrium random velocity along the compressional evolution due to the self-gravity.

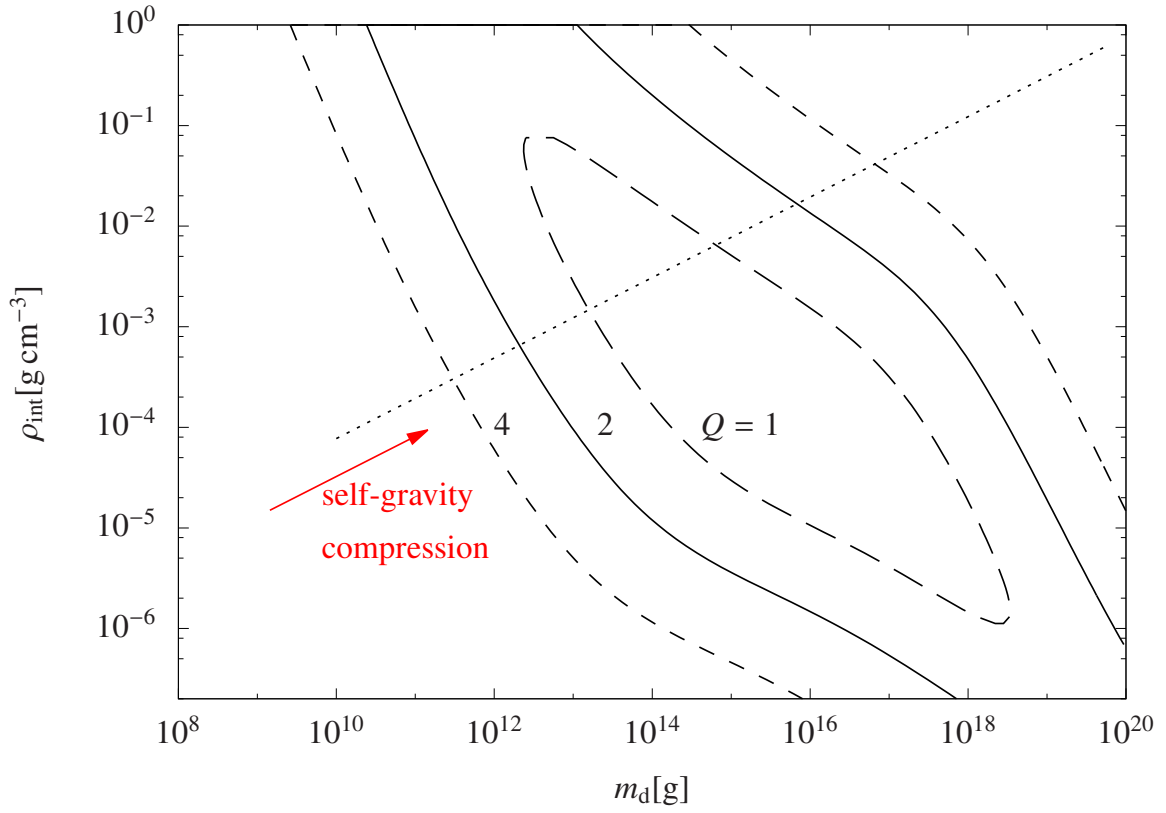


Fig. 1.— GI region on the m_d - ρ_{int} plane at 5 AU for the fiducial model. The dashed, solid, and short-dashed curves show contours for $Q = 1, 2,$ and $4,$ respectively. The dotted line represents the evolution track of dust aggregates by the self-gravitational compression (Kataoka et al. 2013).

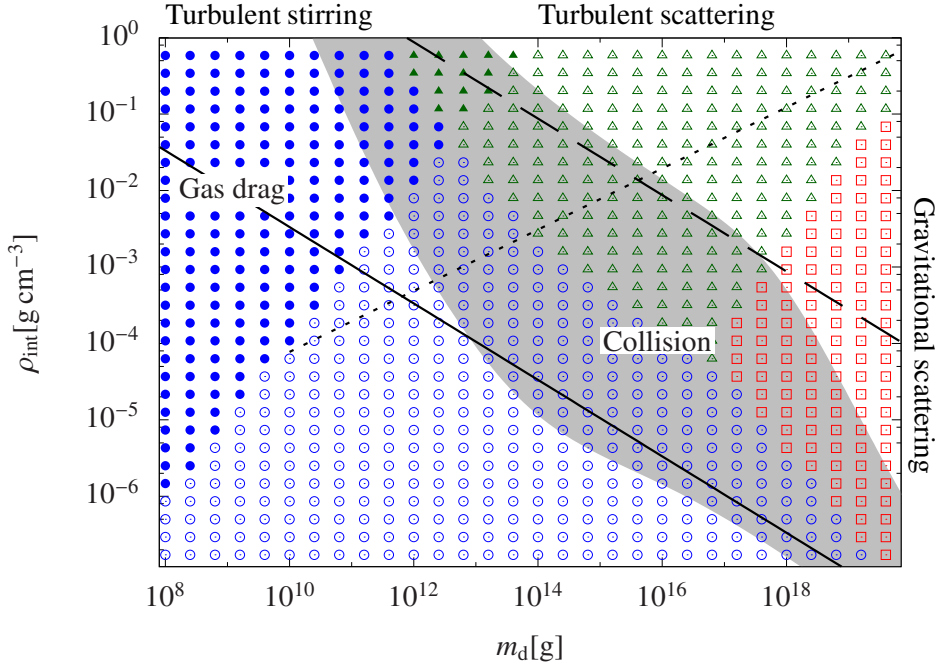


Fig. 2.— Dominant heating and cooling mechanisms for the fiducial model at 5 AU. The filled and open symbols represent gas drag and collisional damping for the dominant cooling process, respectively. The squares, circles, and triangles represent gravitational scattering, turbulent stirring, and turbulent scattering, respectively. The shaded region denotes the GI region where $Q < Q_{\text{crit}}$. The solid and dashed lines represent the approximated instability condition described by Equations (11) and (12), respectively. The dotted line represents the evolution track.

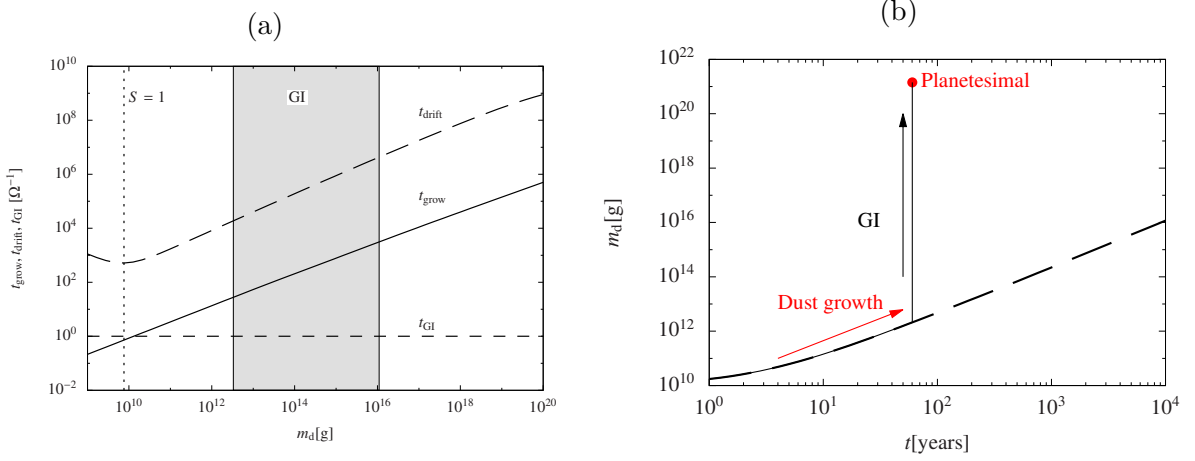


Fig. 3.— (a) Timescales of the dust growth (solid), radial drift (dashed), and GI (short dashed) in the fiducial model at 5 AU. The dotted line and the shaded region correspond to $S = 1$ and the GI region ($Q < Q_{\text{crit}}$), respectively. (b) Time evolution of the dust mass. The dashed curve shows the evolution only by the collisional growth along the evolution track and the solid curve shows the evolution including the GI. The time t means the time elapsed since $m = 10^{10}$ g.

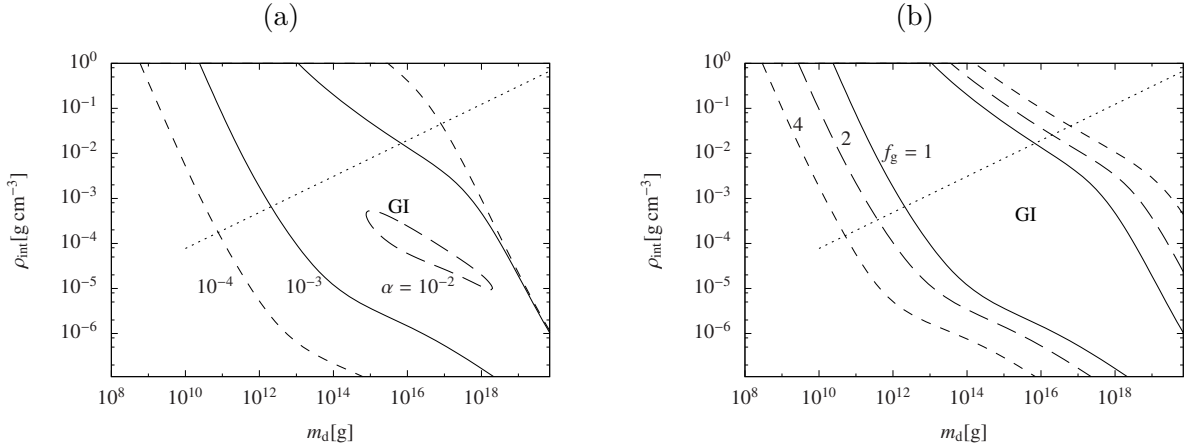


Fig. 4.— Dependence of the GI regions on (a) α and (b) f_g . (a) $\alpha = 10^{-2}$ (dashed), 10^{-3} (solid), and 10^{-4} (short-dashed) with $f_g = 1$. (b) $f_g = 1$ (solid), 2 (dashed), and 4 (short-dashed) with $\alpha = 10^{-3}$. The dotted line is the evolution track.

We calculated the equilibrium random velocity considering gravitational scattering and collisions among dust aggregates, gas drag, and turbulent stirring and scattering. We obtained the ranges of the mass and internal density of dust aggregates for the gravitational instability (GI). We found that in the minimum-mass solar nebula model with turbulence strength $\alpha \lesssim 7 \times 10^{-3}$, the disk becomes gravitationally unstable as the dust aggregates grow. The disk with weaker turbulence (smaller α) and larger mass (larger f_g) is more prone to become gravitationally unstable almost independently of its distance from the central star. For the reasonable ranges of disk parameters the dust evolution inevitably leads to the GI.

When the GI occurs, the dust internal density is still low. The post-GI evolution of the disk of such aggregates was investigated by N -body simulations (Michikoshi et al. 2007, 2009, 2010). They showed that the GI leads to formation of planetesimals with mass on the order of

$$m_{\text{pl}} \simeq \lambda_{\text{cr}}^2 \Sigma_{\text{d}} = 1.42 \times 10^{21} f_g^3 \left(\frac{f_{\text{d}}}{0.018} \right)^3 \left(\frac{a}{5 \text{ AU}} \right)^{3/2} \text{ g}, \quad (15)$$

where $\lambda_{\text{cr}} = 4\pi^2 G \Sigma_{\text{d}} / \Omega^2$ is the critical wavelength of the GI. We propose the GI of the porous-dust disk as a viable mechanism for planetesimal formation. Note that their disk models are rather limited and the further investigation of the post-GI evolution is also necessary.

In the present paper, we adopted the limited disk model and the simple model of the dust aggregate dynamics to see the basic physics as a first step. Using more general disk models and more realistic dynamics we systematically investigate the disk stability and obtain more rigorous GI conditions in the subsequent paper.

REFERENCES

- Adachi, I., Hayashi, C., & Nakazawa, K. 1976, *Progress of Theoretical Physics*, 56, 1756
- Blum, J. & Wurm, G. 2000, *Icarus*, 143, 138
- Brown, P. P. & Lawler, D. F. 2003, *Journal of Environmental Engineering*, 129, 222
- Chiang, E. & Youdin, A. N. 2010, *Annual Review of Earth and Planetary Sciences*, 38, 493
- Cuzzi, J. N., Hogan, R. C., Paque, J. M., & Dobrovolskis, A. R. 2001, *ApJ*, 546, 496
- Dominik, C. & Tielens, A. G. G. M. 1997, *ApJ*, 480, 647
- Goldreich, P. & Ward, W. R. 1973, *ApJ*, 183, 1051
- Hayashi, C. 1981, *Progress of Theoretical Physics Supplement*, 70, 35
- Hayashi, C., Nakazawa, K., & Nakagawa, Y. 1985, 1100
- Ida, S. 1990, *Icarus*, 88, 129

- Inaba, S., Tanaka, H., Nakazawa, K., Wetherill, G. W., & Kokubo, E. 2001, *Icarus*, 149, 235
- Johansen, A., Oishi, J. S., Low, M.-M. M., Klahr, H., Henning, T., & Youdin, A. 2007, *Nature*, 448, 1022
- Kataoka, A., Tanaka, H., Okuzumi, S., & Wada, K. 2013, *A&A*, 557, L4
- Kokubo, E. & Ida, S. 1998, *Icarus*, 131, 171
- . 2012, *Progress of Theoretical and Experimental Physics*, 2012, 01A308
- Michikoshi, S. & Inutsuka, S.-i. 2006, *ApJ*, 641, 1131
- Michikoshi, S., Inutsuka, S.-i., Kokubo, E., & Furuya, I. 2007, *ApJ*, 657, 521
- Michikoshi, S. & Kokubo, E. 2016, *ApJ*, 821, 35
- Michikoshi, S., Kokubo, E., & Inutsuka, S. 2010, *ApJ*, 719, 1021
- Michikoshi, S., Kokubo, E., & Inutsuka, S.-i. 2009, *ApJ*, 703, 1363
- . 2012, *ApJ*, 746, 35
- Okuzumi, S. & Ormel, C. W. 2013, *ApJ*, 771, 43
- Okuzumi, S., Tanaka, H., Kobayashi, H., & Wada, K. 2012, *ApJ*, 752, 106
- Okuzumi, S., Tanaka, H., Takeuchi, T., & Sakagami, M.-a. 2011, *ApJ*, 731, 96
- Safronov, V. 1969
- Salo, H. 1995, *Icarus*, 117, 287
- Sano, T., Miyama, S. M., Umebayashi, T., & Nakano, T. 2000, *ApJ*, 543, 486
- Sekiya, M. 1998, *Icarus*, 133, 298
- Sekiya, M. & Ishitsu, N. 2000, *Earth, Planets, and Space*, 52, 517
- Stewart, G. R. & Ida, S. 2000, *Icarus*, 143, 28
- Suyama, T., Wada, K., & Tanaka, H. 2008, *ApJ*, 684, 1310
- Suyama, T., Wada, K., Tanaka, H., & Okuzumi, S. 2012, *ApJ*, 753, 115
- Takahashi, S. Z. & Inutsuka, S.-i. 2014, *ApJ*, 794, 55
- Toomre, A. 1964, *ApJ*, 139, 1217
- . 1981, *Structure and Evolution of Normal Galaxies* (Cambridge: Cambridge Univ. Press), 111

Wada, K., Tanaka, H., Suyama, T., Kimura, H., & Yamamoto, T. 2007, *ApJ*, 661, 320

—. 2008, *ApJ*, 677, 1296

—. 2009, *ApJ*, 702, 1490

Weidenschilling, S. J. 1977, *MNRAS*, 180, 57

Weidenschilling, S. J. & Cuzzi, J. N. 1993, 1031

Youdin, A. N. 2011, *ApJ*, 731, 99

Youdin, A. N. & Goodman, J. 2005, *ApJ*, 620, 459

Youdin, A. N. & Lithwick, Y. 2007, *Icarus*, 192, 588

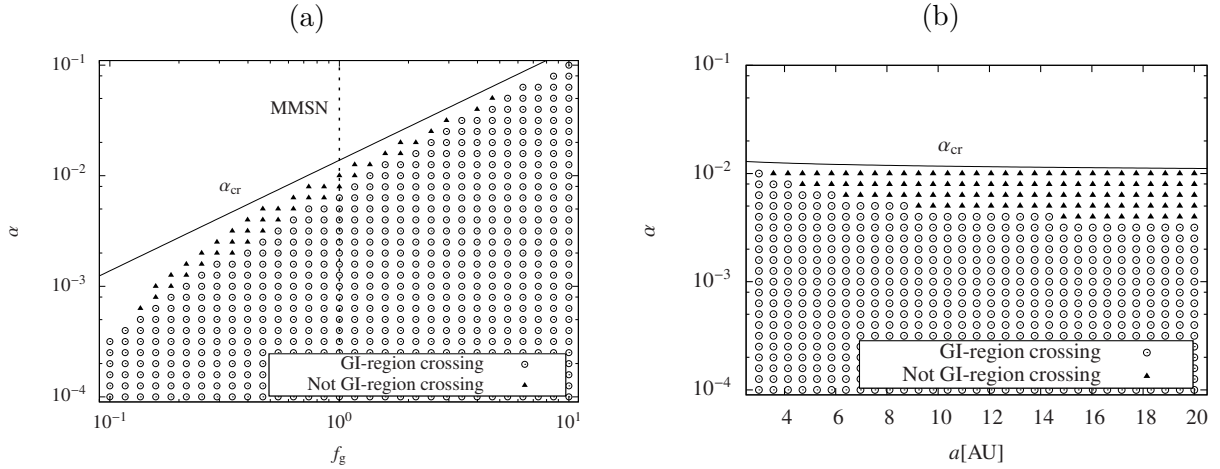


Fig. 5.— Parameter regime for the GI on the f_g - α plane at $a = 5$ AU (a) and on the a - α plane with the MMSN model $f_g = 1$ (b). The points show the cases where the GI region exists in the area $10^8 < m_d < 10^{20}$ g and $10^{-6} \text{ g cm}^{-3} < \rho_{\text{int}} < 1 \text{ g cm}^{-3}$ on the m_d - ρ_{int} plane. The filled triangle represents the case where the evolution track does not cross the GI region. The circle shows the case where the evolution track crosses the GI region. The solid line represents α_{cr} described by Equation (14). The dotted line corresponds to the MMSN model.